Dimensionality-Driven Evolution of Electronic Structure and Transport Properties in Pressure-Induced Phases of Ca$_2$N Electride

M. A. Mazannikova$^{+*\times}$[1], Dm. M. Korotin^{+*}, V. I. Anisimov$^{+*\times}$, A. R. Oganov*, D. Y. Novoselov$^{+*\times}$

$^+$M. N. Mikheev Institute of Metal Physics of Ural Branch of the Russian Academy of Sciences,
620108 Yekaterinburg, Russia

*Skolkovo Institute of Science and Technology, 121205 Moscow, Russia

$^\times$Department of theoretical physics and applied mathematics,
Ural Federal University, 620002 Yekaterinburg, Russia

We investigate how the 2D → 1D → 0D reduction in dimensionality of interstitial electronic states in the Ca$_2$N electride influences its electronic structure and transport properties. Employing the Maximally Localized Wannier Functions (MLWF) approach, we successfully describe the interstitial quasi-atomic states (ISQ) located in non-nuclear Wyckoff positions between Ca atoms. This allowed us to conclude that the electride subsystem is responsible for the formation of the band structure in the vicinity of the Fermi level in all Ca$_2$N phases observed under pressure. Using the obtained MLWF basis, we calculate the electronic and thermal conductivity, along with the Seebeck coefficient, by solving the semi-classical Boltzmann transport equations. The results achieved permit the conclusion that the counterintuitive increase in resistance under pressure observed experimentally is attributed to enhanced localization of interstitial electronic states through the 2D → 1D → 0D electride subspace transformations. We also established a substantial anisotropy in the transport properties within the 2D phase and found that the conductivity inside the plane of the electride layers is provided by electrons, while along the direction normal to the layers, holes become the majority carriers.

1. Introduction. Lately, there has been a notable surge of interest within the scientific community towards a novel category of materials known as inorganic electrides [1–12]. These materials have significant potential to advance the development of artificial materials. Electrides belong to a unique category of ionic compounds where excess electrons are distributed within voids in the crystal structure, taking on the role of anions [13]. The distinctive electronic structure of electrides arises from the loosely bound trapped electrons, resulting in remarkable physical and chemical properties. These properties include high electron mobility, an extremely low work function, strong electron-donating capabilities, and good oxidation and catalytic activity [7, 14]. Such remarkable features of the electronic structure make electrides highly attractive for a wide range of applications, including their use as catalyst promoters or catalysts [15], battery electrode materials [16], electronic devices, superconductors [17], and new magnetic materials [18].

Recently, a Ca$_2$N – layered electride material, characterized by the presence of anionic electrons confined within a two-dimensional domain, has been reported [19]. The chemical formula [Ca$_2$N]$^+$·e$^-$ indicates the existence of anionic electrons distributed in the interstitial space between two Ca-N layers. Earlier research [19] of Ca$_2$N has shown that this material undergoes a sequence of structural phase transitions under external pressure from R$\bar{3}$m phase to Fd$\bar{3}$m phase then to I$\bar{4}$2d and then to Cc. These transitions are accompanied by a gradual decrease in the electride subspace dimension 2D → 1D → 0D. At the same time, experimental measurements of electrical resistance [19] find a transition from the metallic phase to the semiconductor phase during pressure increase. It was previously shown that the localization of interstitial electronic states plays an important role in the formation of the electronic structure of electrides, especially near the Fermi level [12, 20]. Consequently, any changes in the degree of localization can cause significant alterations in the transport properties of the material. This work aims to theoretically study the role of interstitial electronic states in the for-

---

[1]e-mail: mazannikova@imp.uran.ru

mation of the transport properties of Ca_2N such as electronic conductivity, thermal conductivity, and the Seebeck coefficient, as well as their evolution with a decrease in the dimension of the electride subspace. To describe the subspace of electride states, we propose the construction of maximally localized Wannier functions (MLWFs) [21], that are centered in non-nuclear Wyckoff positions. Subsequently, these MLWFs are used as a basis for the wave functions of the electride states to solve the semi-classical Boltzmann transport equations [22].

2. Computational methods. Electronic structure calculations were performed using DFT within the generalized gradient approximation (GGA) and the Perdew–Burke–Ernzerhof (PBE) functional [23] implemented in the QUANTUM ESPRESSO package [24]. Initial crystal structure data for Ca_2N were taken from [19]. Integration in the reciprocal space was performed on a regular $16 \times 16 \times 16$ k-points mesh in the irreducible part of the Brillouin zone. The MLWF basis was obtained using the Wannier90 package [25]. Electronic transport properties were calculated by solving the semiclassical Boltzmann transport equations in the constant relaxation-time approximation using the BoltzWann code [22] embedded in the Wannier90 package [25]. Bader charges [26] were calculated using the Critic2 program [27].

3. Results and discussion.

3.1. Wave functions of interstitial states. Under normal conditions, excess anionic electrons in Ca_2N form 2D electronic layers in the xy plane of the R$\bar{3}$m crystal structure [19]. The band structure in the vicinity of the Fermi level consists of 4 hybridized energy bands, including three p-states of nitrogen and one interstitial electronic state (see Fig. 1). Thus, the basis of the states lying near the Fermi includes 4 MLWFs. The first MLWF corresponding to the electride state is centered at the $3b$ Wyckoff positions and predominantly have an s-like orbital symmetry. The contribution of the first MLWF to the band structure is shown in Fig. 1a in light purple. As can be seen, interstitial electrons mainly occupy a partially filled band crossing the Fermi level and providing the metallicity of this phase. The width of the electride band in this case is about 2 eV. The remaining three MLWFs describe three fully occupied energy bands in the interval $[-3.5; -1.2]$ eV. These bands possess a p-orbital symmetry and are centered on the nitrogen atom. Figure 1a shows that the energy band crossing the Fermi level is predominantly formed by interstitial electronic states, which clearly confirms the assumption that the excess anionic electrons are responsible for the transport properties of this material in the 2D phase.
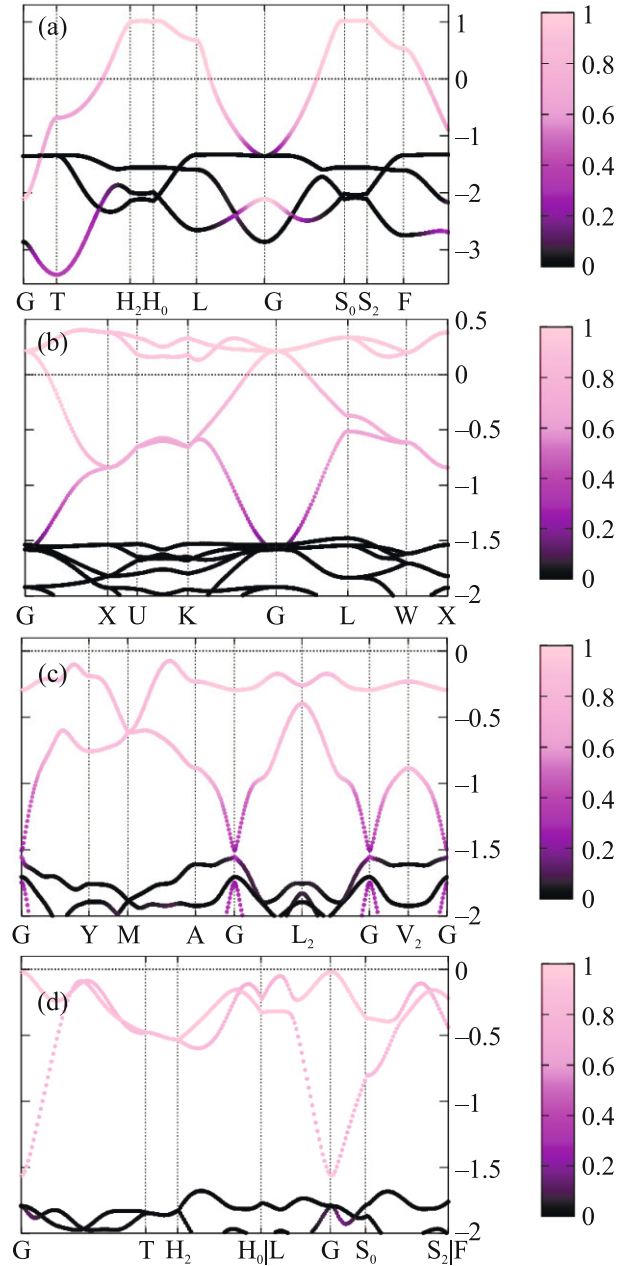

Fig. 1. (Color online) Band structure of Ca_2N relative to the Fermi level (E_F) for: (a) – R$\bar{3}$m; (b) – Fd$\bar{3}$m; (c) – I$\bar{4}$2d; (d) – Cc structures (solid black curves) and MLWFs with colored projected components of interstitial MLWFs

As shown in [19], an increase in pressure to about 12.7 GPa leads to a transition from the R$\bar{3}$m to the Fd$\bar{3}$m phase. This transition is accompanied by a reduction in the subspace's dimensionality, from 2D to 1D. The MLWFs basis for Fd$\bar{3}$m structure includes 16 states, 4 of which correspond to anionic electronic states and are located at the $16c$ Wyckoff positions.
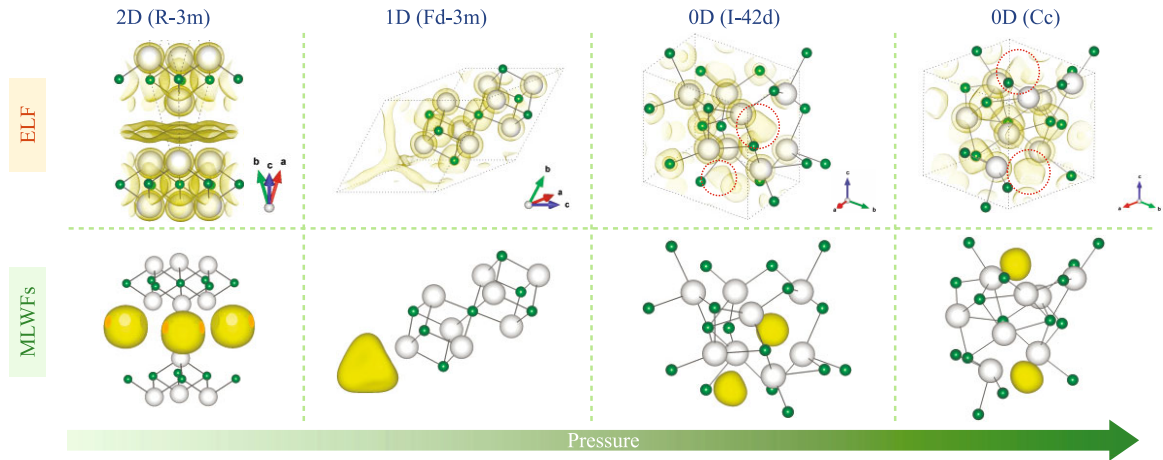
Fig. 2. (Color online) Evolution of ELF and MLWFs isosurfaces of Ca_2N under pressure. The isosurfaces of the electron localization function for $R\bar{3}$, $Fd\bar{3}m$, $I\bar{4}2d$, Cc structures with value 0.55, 0.7, 0.8, and 0.8, respectively. White and green spheres denote Ca and N atoms

The other 12 are fully occupied p-states of the four nitrogen atoms. The contribution of the first four MLWFs to the band structure is shown in Fig. 1b. As can be seen from this figure, the interstitial electronic states make the main contribution to the four energy bands lying in the vicinity of the Fermi level and crossing it. The total width of the electride band for the 1D case is close to that in the 2D phase and is about 2 eV. However, in this case, two subbands with different dispersions are formed in the spectrum of interstitial states: one partially filled has a width of about 1.7 eV, and the second is completely empty with a width of less than 0.5 eV. Such dispersion indicates an increase in the localization of interstitial states during the 2D–1D transition. As in the 2D case, the transport properties in the 1D phase are also determined by interstitial electrons.

A further increase in pressure causes the next transition to the $I\bar{4}2d$ phase at about 20.5 GPa [19]. In this phase, the electride subspace has zero dimension. Another transition also to the 0D electride phase with Cc symmetry occurs at 37.5 GPa [19]. To obtain the basis of MLWFs for $I\bar{4}2d$ and Cc phases, 14 states were projected; the first two correspond to electride states and the other 12 are associated with fully occupied p-states of four N atoms. For $I\bar{4}2d$ structure, the first two WFs were centered at the $4b$ Wyckoff positions. For the crystal structure with Cc symmetry, the first two states were centered at the positions (0.500, 0.750, 0.125), (0.000, 0.125, 0.750). The contribution of interstitial MLWFs to the band structure of $I\bar{4}2d$ and Cc phases is shown in Fig. 1c and d respectively. Both 0D phases have an energy gap and their interstitial states are completely filled, forming the top of the valence band. In both cases, the dispersion of the two available electride bands is

noticeably different. However, the upper band is quite flat and has a width of only about 0.5 eV, which indicates a strong localization of the corresponding electronic states.

Thus, interstitial electronic states make the main contribution to the band structure near the Fermi level in all the considered Ca_2N phases. Changes in the energy band dispersion and a reduction in the dimension of the electride subspace indicate an increase in the degree of localization of these states during phase transitions. These observations imply that the nature of the unusual resistance behavior observed in the experiment, exhibiting an increase with rising pressure, is entirely determined by the properties of the electride electronic subsystem of Ca_2N.

3.2. Spatial distribution of ELF and MLWF. To describe a topology of the spatial distribution of the interstitial charge density and the degree of localization of anionic electrons in varying Ca_2N phases, we calculated both the electron localization function (ELF) [28] and the Bader charges. The search for non-nuclear attractors in Bader basins has enabled the determination of Wyckoff positions for interstitial localization centers. Fig. 2 (upper panel) shows the isosurfaces of the ELF for structures with $R\bar{3}$, $Fd\bar{3}m$, $I\bar{4}2d$, Cc symmetry with the isosurface values 0.55, 0.7, 0.8, and 0.8, respectively.

In the $R\bar{3}m$ crystal structure, anionic electrons form a two-dimensional layer of electronic gas, bounded by calcium atoms. Bader charge calculations reveal the existence of a non-nuclear charge density maximum in the same position as the electride Maximally Localized Wannier Function (MLWF). The MLWFs corresponding to the electride electronic states are depicted in the lower panel of Fig. 2. However, the charge integral within

this Bader basin is extremely low, measuring less than 0.01 electron. This observation finds its rationale in the substantial degree of electron delocalization inherent in this structural configuration.

In the Fd$\bar{3}$m crystal structure, electrons are organized into a continuous one-dimensional charged network. This is evident from the isosurface representation of the ELF (Fig. 2, upper panel). The isosurface of the sum of four resulting electride MLWFs is shown in Fig. 2. Their spatial distribution resembles the region of the ELF that coincides with the junction of the one-dimensional chains. The calculated Bader charge amounts to 1.5 electrons (0.375 per formula unit), significantly exceeding the value observed in the R$\bar{3}$m phase. This outcome signifies a noticeable enhancement in the level of interstitial state localization within the 1D phase compared to the 2D phase.

The ELF isosurface distribution, as illustrated in Fig. 2, reveals that structures possessing I$\bar{4}$2d and Cc symmetry exhibit regions of charge density in zero dimensions (0D). The spatial arrangement of the Maximally Localized Wannier Functions (MLWFs) in these structures bears resemblance to the ELF isosurfaces. The calculated Bader basin charges for the I$\bar{4}$2d and Cc structures amount to 1.5 (0.374 per formula unit) and 1.3 (0.325 per formula unit) electrons, respectively.

Therefore the analysis of changes in the ELF isosurface as well as the shape and spatial distribution of the MLWFs confirms that the structural transitions induced by pressure in Ca$_2$N are accompanied by a stepwise reduction in the dimensionality of the subspace occupied by anionic electrons, whose states can be effectively analytically described through MLWFs centered at the corresponding interstitial sites of the crystal lattice.

3.3. Electrical conductivity. Subsequently, in order to determine the transport properties of Ca$_2$N within each phase, we employed the obtained MLWF basis sets corresponding to the electride states to solve semi-classical Boltzmann equations. The plots illustrating the dependence of electrical conductivity divided by relaxation time with respect to chemical potential for the R$\bar{3}$m, Fd$\bar{3}$m, I$\bar{4}$2d, and Cc structures at three constant temperatures (100, 200, and 300 K) are depicted in Fig. 3. It is clear from the figure that the electrical conductivity at the Fermi level is highest for the R$\bar{3}$m phase among the structures considered. It increases with electron doping and exhibits a peak around a chemical potential of approximately 0.4 eV, associated with the maximum electronic capacity of the electride layer. As expected, hole doping leads to a decrease in electrical conductivity, which is attributed to the reduction in the charge carrier concentration within the interstitial layers. The
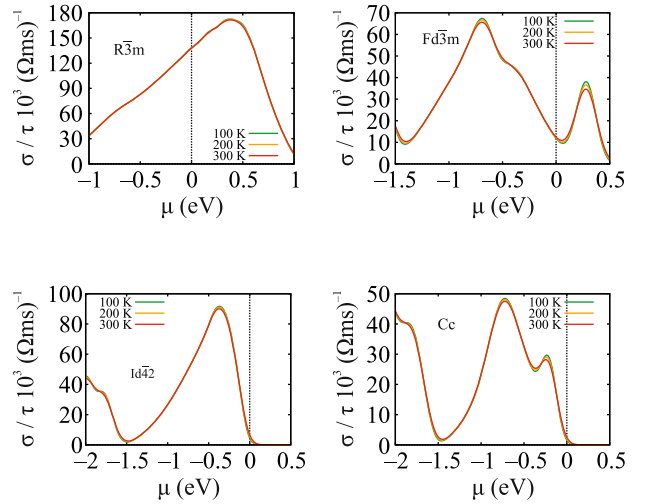

Fig. 3. (Color online) Electrical conductivity relative to relaxation time as a function of chemical potential at three constant temperatures 100, 200 and 300 K for R$\bar{3}$m, Fd$\bar{3}$m, I$\bar{4}$2d, Cc structures

transition from 2D to 1D configuration is concomitant with a notable reduction in electrical conductivity by a factor of several magnitudes. However, electron doping in the 1D phase may lead to an approximately three-fold increase in conductivity, as this phase exhibits a peak in the electron doping region attributed to the presence of additional electronic capacity within the 1D-channel electride chains. In the 0D phases, since DFT calculations predict an energy gap and the interstitial states are fully occupied, the obtained solution corresponds to an insulator. Consequently, the computation of electrical conductivity based on the interstitial wave function basis reproduces the observed decline in electrical conductivity as seen in experiments [19].

The decrease in conductivity with an increase in external pressure is an atypical behavior for most metals, except for certain alkali metals (Li, K, and Na) [29–32]. The nature of this unusual phenomenon lies in the peculiarities of electronic states in the vicinity of the Fermi level. In electrides, these states correspond to electrons detached from atoms and located in periodic crystalline voids. An increase in pressure leads to compression of the spatial region of their confinement, resulting in enhanced localization. Additionally, it causes an increase in Coulomb repulsion between excess electrons. This effect is particularly pronounced during the 1D-0D transition from the connected to disconnected topology of the charge density, which is accompanied by a sharp jump in resistance and the opening of an energy gap.

Also, it can be observed from Fig. 3 that the change in temperature does not have a significant influence on

electrical conductivity. This contradicts experimental observations [19], which indicate a significant temperature dependence of resistance, especially in the two-dimensional and zero-dimensional phases. The discrepancy may be attributed to the fact that the computational method used in this study does not account for the temperature effects of atomic vibrations in the crystalline lattice.

The conductivity of the 2D structure with R$\bar{3}$m symmetry shows high directional anisotropy (Fig. 4 upper panel). The in-plane component of σ is an order of magnitude greater than the out-of-plane conductivity at 300 K. Such behavior results from the substantial anisotropy of the two-dimensional electride subsystem which determines the dispersion of electronic energy states directly at the Fermi level and in its vicinity.
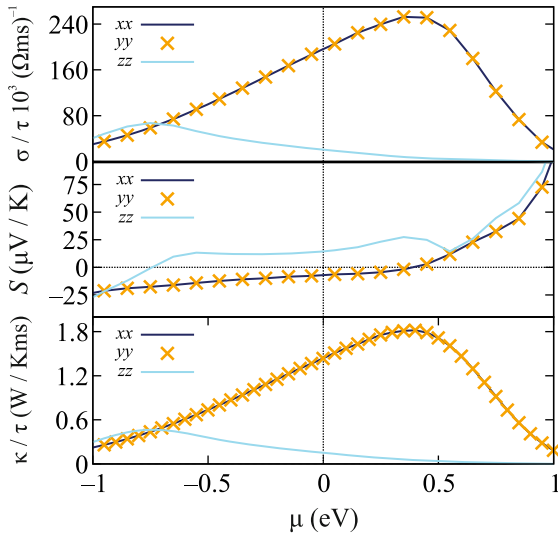

Fig. 4. (Color online) Dependence of electrical conductivity relative to relaxation time, Seebeck coefficient and electronic thermal conductivity relative to relaxation time on chemical potential at 300 K for R$\bar{3}$m structure

3.4. Seebeck coefficient. The Seebeck coefficient can be positive or negative, and its sign indicates the type of majority charge carriers: $+S$ represents p-type materials, i.e. positive charge carriers (holes), while n-type materials are denoted by $-S$ [33].

The dependencies of the Seebeck coefficient on the chemical potential for R$\bar{3}$m, Fd$\bar{3}$m, I$\bar{4}$2d and Cc structures at three temperatures (100, 200 and 300 K) are shown in Fig. 5. It is evident that the Seebeck coefficient at E_F is positive for each of the phases, indicating that holes act as the primary charge carriers. We observe an increase in the Seebeck coefficient during the transition from the metallic state to the semiconductor state, which is characteristic of decreased charge car-
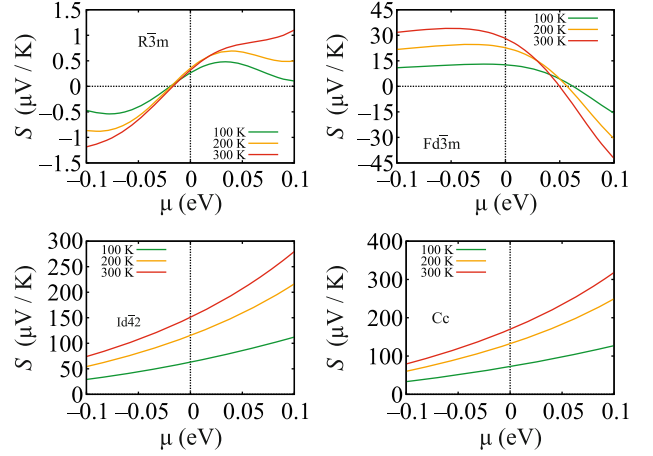

Fig. 5. (Color online) Seebeck coefficient as a function of chemical potential at three constant temperatures 100, 200 and 300 K for R$\bar{3}$m, Fd$\bar{3}$m, I$\bar{4}$2d, Cc structures

rier concentration [34]. In the Fd$\bar{3}$m structure, electron doping can alter the majority carrier type, leading to increased electrical conductivity.

In the 2D phase of Ca$_2$N, similar to its electrical conductivity, the Seebeck coefficient exhibits notable anisotropy. The dependence of the components S_{xx}, S_{yy}, S_{zz} of the Seebeck coefficient on the chemical potential for the R$\bar{3}$m structure is illustrated in Fig. 4 (middle panel). The values of the Seebeck coefficient in the xy plane are negative, indicating that electrons are the majority charge carriers within the electride layers. Conversely, along the normal direction of these layers, holes serve as the majority carriers.

3.5. Electronic thermal conductivity. The most effective thermoelectric materials are those with low thermal conductivity. Thermal conductivity usually consists of two parts: the electronic part (k_e), in which the electrons and holes are responsible for transporting heat, and the phonon part (k_l), where the phonons travel through the lattice. We should emphasize that the BoltzWann code allows us to calculate only the electronic part k_e. Fig. 6 represents the electronic thermal conductivity of the analyzed structures as a function of chemical potential at three constant temperatures (100, 200 and 300 K).

For a 2D structure, the thermal conductivity is noticeably higher than for the others, and it also has a strong temperature dependence. This behavior is explained by the presence of a bound region in the xy plane (Fig. 4) of almost free electrons, which act as a medium for the transfer of thermal energy. The picture is similar for a 1D structure, but the thermal conductivity is considerably lower. The thermal conductivity of 0D phases exhibits a reverse dependence, resulting in lower thermal conductivity and less temperature de-
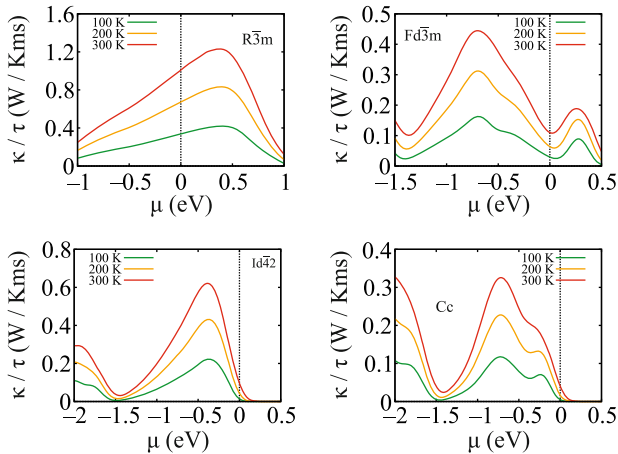
Fig. 6. (Color online) Electronic thermal conductivity relative to relaxation time as a function of chemical potential at three constant temperatures 100, 200 and 300 K for R$\bar{3}$m, Fd$\bar{3}$m, I$\bar{4}$2d and Cc structures

pendence. The anisotropy of the thermal conductivity for a 2D structure arises for the same reason as the electrical conductivity. In the I$\bar{4}$2d and Cc phases, the electronic subsystem does not contribute to the thermal conductivity under electron doping, since both phases have an energy gap. Therefore, the electronic thermal conductivity of Ca$_2$N, similar to its electrical conductivity, shows a notable trend of a sharp decrease with increasing pressure.

4. Conclusion. In conclusion, we have investigated the contribution of interstitial electronic states to the electronic structure and transport properties of Ca$_2$N in its 2D, 1D, and 0D electride phases arising under pressure. By analyzing the Electron Localization Function, we determined the Wyckoff positions of interstitial quasi-atoms. For each phase, we employed an approach involving the construction of a maximally localized Wannier function basis centered at these nonnuclear positions. This enabled the rigorous identification of the electride states contributions to the band structure of Ca$_2$N, leading to a conclusion regarding their crucial role in shaping the transport properties of all pressure-induced phases of Ca$_2$N. The study revealed that the counterintuitive increase in resistance driven by pressure, as observed experimentally [19], is rooted in the enhanced localization of interstitial electronic states that takes place with the 2D $\rightarrow$ 1D $\rightarrow$ 0D dimensionality reduction of the electride subsystem. Across all phases of Ca$_2$N, a positive Seebeck coefficient is observed, signifying that holes are the majority carriers. However, for the 2D phase, it was found that the Seebeck coefficient within the plane of electride layers is negative, indicating that conductivity within the plane is governed by electrons, while along the normal direction to the

layers, holes become the majority carriers. It has been established that a decrease in the dimensionality of the electrid subspace also leads to a decrease in electronic thermal conductivity, and the transition to a 0D phase results in a sharp decline. Thus, our findings reveal that the transport properties of the Ca$_2$N electride are governed by electronic states described by interstitial wave functions.

1. P. P. Edwards, Science **333**, 49 (2011).
2. Q. Zhu, T. Frolov, and K. Choudhary, Matter **1**, 1293 (2019).
3. D. Y. Novoselov, D. M. Korotin, A. O. Shorikov, A. R. Oganov, and V. I. Anisimov, JETP Lett. **109**, 387 (2019).
4. D. Y. Novoselov, D. M. Korotin, A. O. Shorikov, A. R. Oganov, and V. I. Anisimov, J. Phys.: Condens. Matter **32**, 445501 (2020).
5. D. Y. Novoselov, D. M. Korotin, A. O. Shorikov, V. I. Anisimov, and A. R. Oganov, J. Phys. Chem. C **125**, 15724 (2021).
6. D. Y. Novoselov, V. I. Anisimov, and A. R. Oganov, Phys. Rev. B **103**, 235126 (2021).
7. H. Hosono and M. Kitano, Chem. Rev. **121**, 3121 (2021).
8. Z. Wan, W. Xu, T. Yang, and R. Zhang, Phys. Rev. B **106**, L060506 (2022).
9. S. Liu, C. Wang, H. Jeon, Y. Jia, and J. H. Cho, Phys. Rev. B **105**, L220401 (2022).
10. Z. Liu, Q. Zhuang, F. Tian, D. Duan, H. Song, Z. Zhang, and T. Cui, Phys. Rev. Lett. **127**, 157002 (2021).
11. A. Fujimori, Nat. Mater. **21**, 1217 (2022).
12. M. A. Mazannikova, D. M. Korotin, A. O. Shorikov, V. I. Anisimov, and D. Y. Novoselov, J. Phys. Chem. C **127**, 8714 (2023).
13. K. Lee, S. W. Kim, Y. Toda, S. Matsuishi, and H. Hosono, Nature **494**, 336 (2013).
14. X. Zhang and G. Yang, Phys. Chem. Lett. **11**, 3841 (2020).
15. J. Li, S. Inagi, T. Fuchigami, H. Hosono, and S. Ito, Electrochem. Commun. **44**, 45 (2014).
16. T. Kocabas, A. Ozden, I. Demiroglu, D. Çakır, and C. Sevik, J. Phys. Chem. Lett. **9**, 4267 (2018).
17. B. Sa, R. Xiong, C. Wen, Y. L. Li, P. Lin, Q. Lin, and Z. Sun, J. Phys. Chem. C **124**, 7683 (2020).

18. D. Liu and D. Tomanek, Nano Lett. **19**, 1359 (2019).

19. H. Tang, B. Wan, B. Gao et al. (Collaboration), Adv. Sci. **5**, 1800666 (2018).

20. D. Y. Novoselov, M. A. Mazannikova, D. M. Korotin, A. O. Shorikov, M. A. Korotin, V. I. Anisimov, and A. R. Oganov, J. Phys. Chem. Lett. **13**, 7155 (2022).

21. I. Souza, N. Marzari, and D. Vanderbilt, Phys. Rev. B **65**, 035109 (2001).

22. G. Pizzi, D. Volja, B. Kozinsky, M. Fornari, and N. Marzari, Comput. Phys. Commun. **185**, 422 (2014).

23. J. P. Perdew, K. Burke, and M. Ernzerhof, Phys. Rev. Lett. B **77**, 3865 (1996).

24. P. Giannozzi, S. Baroni, N. Bonini et al. (Collaboration), Phys. Condens. Matter. **21**, 395502 (2009).

25. A. A. Mostofi, J. R. Yates, G. Pizzi, Y.-S. Lee, I. Souza, D. Vanderbilt, and N. Marzari, Comput. Phys. Commun. **185**, 2309 (2014).

26. R. F. Bader, Chem. Rev. **91**, 893 (1991).

27. A. Otero-de-la-Roza, E. R. Johnson, and V. Luaña, Comp. Phys. Commun. **185**, 1007 (2014).

28. A. Savin, R. Nesper, S. Wengert, and T. F. Fässler, Angew Chem. Int. Ed. Engl. **36**, 1808 (1997).

29. Y. Ma, M. Eremets, A. R. Oganov, Y. Xie, I. Trojan, S. Medvedev, and V. Prakapenka, Nature **458**, 182 (2009).

30. T. Matsuoka and K. Shimizu, Nature **458**, 186 (2009).

31. T. Yabuuchi, Y. Nakamoto, K. Shimizu, and T. Kikegawa, J. Phys. Soc. Jpn. **74**, 2391 (2005).

32. N. W. Ashcroft, Nature **458**, 158 (2009).

33. S. Kasap, *Thermoelectric effects in metals: thermocouples*, Department of Electrical Engineering University of Saskatchewan, Canada (2001).

34. D. M. Rowe, *CRC handbook of thermoelectrics: macro to nano*, RC, Boca Raton, FL. (2006).